Journal of Materials Chemistry A

RSC Publishing

PAPER

View Article Online
View Journal | View Issue

Mo_3Sb_7 as a very fast anode material for lithium-ion and sodium-ion batteries†

Cite this: *J. Mater. Chem. A*, 2013, **1**, 11163

Loïc Baggetto,*[a] Eric Allcorn,[b] Raymond R. Unocic,[a] Arumugam Manthiram[b] and Gabriel M. Veith*[a]

Mo_3Sb_7 thin films prepared by magnetron sputtering are evaluated as an anode material for Li-ion and Na-ion batteries. The as deposited films are amorphous and composed of small agglomerated domains with an overall Sb/Mo ratio of 2.34 that is almost identical to the ratio measured for the starting powder and the expected nominal ratio of 2.33. When cycled with Li and Na, the films show large storage capacities of around 430 and 330 mA h g^{-1}, respectively, with good capacity retention. In addition, micron thick films retain large capacities of about 310 and 280 mA h g^{-1} at very high rates of 100 and 30 C-rate currents for Li and Na, respectively. The XRD study of the changes in the structure of the electrode material reveals that Li_3Sb forms at full discharge whereas the electrode at full charge is amorphous. For the reaction with Na, the electrode material remains amorphous. Analysis of the surface chemistry characterized by XPS suggests the formation of an inorganic layer (LiF, $Li_xPO_yF_z$) covered by organic products (carbonates, esters, ethers) in the case of Li and the formation of an organic layer only (carbonates) in the case of Na. The electrode surface is visible at full charge for Na, thereby indicating that the Solid Electrolyte Interphase (SEI) layer is thinner when cycling with Na compared to that with Li. Overall, the results highlight the very good potential of Mo_3Sb_7 as an anode for Li- and Na-ion batteries.

Received 23rd May 2013
Accepted 1st August 2013

DOI: 10.1039/c3ta12040f

www.rsc.org/MaterialsA

1 Introduction

The success of lithium-ion batteries is intimately related to their outstanding combination of properties in terms of high energy density, long cycle life, safety, and high rate performance.[1] The dominance of lithium-ion batteries is evident over a wide range of applications such as autonomous micro-devices relying on thin film and 3D micro-battery designs, as well as cell phones, laptops, hybrid and full electric vehicles based on conventional battery designs.[1] The study of alternative energy storage technologies has drawn a lot of attention recently for large scale static applications rather than portable electronics or automotive applications.[2,3] The Na-ion battery system is of particular interest to provide low cost and sustainable energy storage solutions.[2–4] Moreover, the energy density expected for Na-ion electrode materials is not expected to be severely impacted by the Na/Na^+ redox potential, which is only about 0.3 V higher than that of Li/Li^+.[2–4] Numerous studies on suitable cathode materials have been reported; in contrast the chemistries suited to store Na on the anode side have been scarcer. Compounds such as $Na_2Ti_3O_7$[5] and hard carbons[6,7] were identified as active for Na-ion reaction but suffer from relatively small storage capacities and slow reaction kinetics.[5–7] Recent advances in the study of metals and intermetallics are offering great promises to boost the energy storage and kinetics of the anodes.[8–15] Antimony[8–10] and tin[11] have attracted a lot of interest in their pure form due to high storage capacities of 660 and 847 mA h g^{-1}, respectively, corresponding to the formation of Na_3Sb and $Na_{15}Sn_4$.

Alloys of Sn and Sb, such as SnSb,[12,13] Cu_2Sb[14] and Cu_6Sn_5,[15] have also attracted increasing attention due to their improved cycling and rate performances. Such intermetallics are in principle excellent candidates as substitutes to the pure elemental electrodes since they are expected to provide better capacity retention.[16] The improvement in capacity retention originates from the lower volume changes or the presence of the inactive element, which can provide a more stable structure and more efficient electronic conduction within the expanding/shrinking framework.[12–16] One such candidate is Mo_3Sb_7, which is a superconductor at very low temperatures (2.2 K)[17] and has shown to possess good capacity retention and low operating voltages (0.9 V) *versus* Li.[16] Assuming the full conversion of Mo_3Sb_7 into 3Mo and $7M_3Sb$ (M = Li or Na), this electrode material should theoretically be able to deliver a reversible storage capacity of 494 mA h g^{-1} equivalent to 4273 mA h cm^{-3}, which is close to the volumetric storage capacity of pure Sb (4422 mA h cm^{-3}).

The present contribution explores for the first time the electrochemical potential profiles, cycling and rate

[a]*Materials Science and Technology Division, Oak Ridge National Laboratory, 1 Bethel Valley Rd., Oak Ridge, TN 37831, USA. E-mail: baggettol@ornl.gov; veithgm@ornl.gov*
[b]*Electrochemical Energy Laboratory & Materials Science and Engineering Program, The University of Texas at Austin, Austin, TX, 78712 USA*

† Electronic supplementary information (ESI) available. See DOI: 10.1039/c3ta12040f

performance of Mo_3Sb_7 thin film electrodes during the electrochemical reaction with Li and Na. The starting material has been characterized in detail using scanning electron microscopy (SEM) combined with energy dispersive X-ray (EDX) spectroscopy analysis and transmission electron microscopy (TEM) with selected area electron diffraction (SAED). For the study of the electrode properties, galvanostatic cycling at various currents ranging from C/10 to 100 C was conducted on identical electrodes in order to reveal the intrinsic differences in reaction thermodynamics and kinetics of Mo_3Sb_7 material during the reaction with respect to Li and Na ions. Moreover, the changes in bulk structure and the evolution of the surface chemistry are reported for the first time using X-ray diffraction (XRD) and X-ray photoelectron spectroscopy (XPS) for both electrochemical systems as a function of voltage.

2 Experimental

Samples preparation

Stoichiometric amounts of Mo (Sigma-Aldrich, 99.9%) and Sb (Sigma-Aldrich, 99.5%) powders were intimately mixed and heated to 780 °C for 18 h in a reducing atmosphere of flowing 95% Ar–5% H_2. The resulting material was ground to produce a uniform powder of Mo_3Sb_7. Each powder batch underwent phase analysis with a Philips XRD system with Cu K_α radiation, and the experimental patterns matched the expected $Im\bar{3}m$ cubic structure of Mo_3Sb_7 (Fig. S1†). The resulting powder was pressed into a 2″ diameter disk and used as the sputtering target. Thin film deposition was carried out onto roughened Cu foils by means of DC magnetron sputtering in Ar plasma. Deposition conditions were 30 W power, 15 mTorr pressure, and 5 cm target–substrate distance. After preparation, the samples were stored inside an Ar-filled glovebox.

Characterization

Electrochemical characterization was conducted at 25 °C with 2-electrode 2032 coin cells (Hohsen, Japan) prepared inside an Ar-filled glovebox. The cells consisted of pure Na (Sigma-Aldrich) or Li (Alfa Aesar) as counter electrodes, glass fiber separators impregnated with 1 M $NaClO_4$ in PC (Sigma-Aldrich) or 1.2 M $LiPF_6$ in dimethyl carbonate (DMC) and EC (Novolyte) electrolyte solutions, and Mo_3Sb_7 thin films as working electrodes. When specified, 5 wt% of anhydrous fluoroethylene carbonate (FEC, Sigma-Aldrich) was added to the Na electrolyte. Galvanostatic cycling was performed on a Maccor 4000 series for electrodes with a surface area of 1.27 cm^2. Electrodes were subjected to low (40 μA cm^{-2}) and high (630 μA cm^{-2}) current cycling. At high current, the discharges were performed with a constant current step of 630 μA cm^{-2} followed by a potential hold at 0.005 V till the current decreased below 157 μA cm^{-2} whereas the charges were conducted at 630 μA cm^{-2}. For *ex situ* characterizations, specimens were extracted from coin cells inside an Ar-filled glovebox and rinsed with anhydrous DMC for XPS or pressed onto a fiber paper to remove the excess electrolyte for XRD.

A Philips diffractometer equipped with Cu K_α radiation and Ni filter was used for XRD data collection. For *ex situ* measurements, cycled thin film electrodes were sealed with a Kapton tape onto a glass slide. SEM micrographs were acquired on a thick film deposited onto roughened Cu foil using Hitachi S-4800 Field Emission SEM. EDX spectra were measured in the same run over multiple areas on the thin films and starting powder using a JEOL JSM-6500F Field Emission SEM equipped with an EDAX detector. TEM and SAED were characterized on a 30 nm thick film deposited onto an electron transparent SiN_x-membrane of a TEM chip using Hitachi HF3300 operated at 300 kV.

Surface chemistry was probed with a PHI 3056 XPS spectrometer equipped with Al and Mg K_α sources (1486.6 and 1253.6 eV). Samples were inserted into the XPS chamber with an air-tight vacuum transfer system. High resolution scans were acquired at 350 W, 23.5 eV constant pass energy, and 0.05 eV energy step, and survey scans were performed at 350 W, 93.9 eV constant pass energy, and 0.3 eV energy step. The binding energies were adjusted by setting the adventitious carbon signal to 284.8 eV.

3 Results and discussion

Structural data of the as-prepared thin films obtained by electron microscopy and electron diffraction are presented in Fig. 1. The films are composed of small agglomerated domains (Fig. 1a) with a surface morphology that follows the roughened Cu substrate (Fig. S2†). According to the EDX chemical analysis collected over three different areas of the film, the average Sb/Mo ratio is estimated to be 2.34. This value matches well with the composition determined for the starting powder (2.32) and the expected composition of Mo_3Sb_7 crystal structure (Fig. S1†). The diffuse rings measured with SAED, during TEM characterization of the Mo_3Sb_7 thin film deposited on a SiN_x membrane, indicates that the films are amorphous. The amorphous nature of the thin films is further confirmed by XRD analysis (see discussion of Fig. 5).

The electrochemical potential profiles and corresponding derivative curves of Mo_3Sb_7 film electrodes during the first two cycles for the reaction with Li and Na are presented in Fig. 2. The reaction with Li during the first discharge (Li-ion insertion) proceeds on a short flat plateau near 0.75 V followed by a sloping plateau centered around 0.65 V, as suggested by the derivative curves (inset). During the second discharge, the profile is now characterized by a sloping plateau around 0.85 V, which indicates that the structure of the charged material is significantly different than the starting material. Both charges (Li-ion removal) are represented by a sloping plateau (broad peak) near 1 V. From an electrochemical point of view, the reaction after one cycle is similar to that of Mo_3Sb_7–C composite powder electrodes,[16] which supports that the atomic short range ordering of the cycled amorphous Mo_3Sb_7 film electrode is similar to that of cycled crystalline Mo_3Sb_7 powder electrode. For the reaction with Na, the first discharge (Na-ion insertion) is characterized by a wide flat plateau near 0.4 V whereas the second discharge has two notable sloping plateaus around 0.7

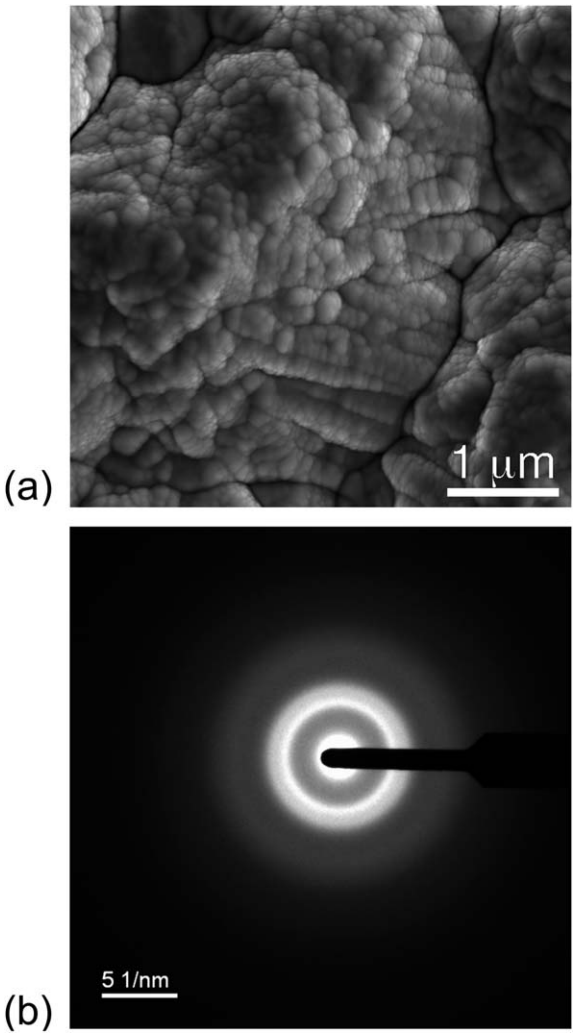

Fig. 1 Properties of the starting Mo_3Sb_7 thin films characterized by electron microscopy: (a) representative scanning electron microscope photograph of a film deposited onto roughened Cu foil and (b) selected area electron diffraction pattern of a 30 nm thick film deposited onto an electron transparent SiN_x membrane for TEM characterization.

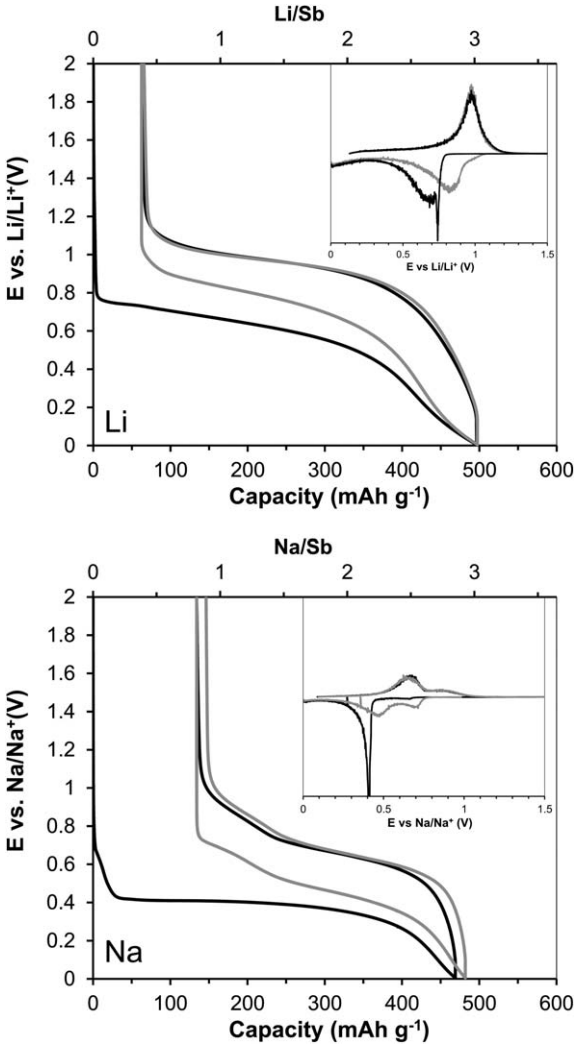

Fig. 2 Electrochemical potential profiles of 1 μm thick Mo_3Sb_7 film electrodes during the first two cycles measured at 40 μA cm^{-2} (C/9 for Li and C/7 for Na). The insets present the corresponding derivative curves of the charge with respect to potential. Black and gray curves are for the first and second cycles, respectively.

and 0.5 V. During both charges (Na-ion removal), the reaction is represented by two sloping plateaus around 0.65 and 0.85 V (Fig. 2). Based on the potential profile during the second cycle, we expect the discharge plateaus (reduction peaks) at 0.5 and 0.7 V to be related to the charge plateaus (oxidation peaks) at 0.65 and 0.85 V, respectively. The important difference in potential profiles during the first and second discharge may be related to a difference in particle size improving the kinetics,[10] or changes in microstructure.[8,13,14]

The initial discharge (ion insertion) capacities for Li and Na are around 500 and 470 mA h g^{-1} and reversible capacities (ion removal) amount to about 430 and 330 mA h g^{-1}, respectively, which correspond to 3719 and 2854 mA h cm^{-3} volumetric capacity based on Mo_3Sb_7 weight density of 8.65 g cm^{-3}. The discharge capacities are close to the theoretical value of 494 mA h g^{-1} (4273 mA h cm^{-3}), which is expected for Mo_3Sb_7 based on the full conversion of Mo_3Sb_7 into $3Mo + 7M_3Sb$ (M = Li or Na). The lower than expected reversible capacities, especially for Na, are likely a result from the trapping of some of the alkali metal, as has been evidenced for pure Sb[8,10] and Cu_2Sb.[14] Compared to a former work on Mo_3Sb_7/C having overall close to 30 wt% C and showing storage capacities of 1500 mA h cm^{-3},[16] the present results are superior. For comparison, Sb can react in practice up to 660 and 550 mA h g^{-1} (ref. 8–10) with Li and Na, respectively, corresponding to 4422 and 3685 mA h cm^{-3} based on Sb weight density of 6.70 g cm^{-3}. $Na_2Ti_3O_7$ (ref. 5) or hard carbons[6,7] have much lower Na storage capacities, well below 1000 mA h cm^{-3}. Sn has much higher storage capacities (847 mA h g^{-1} and 6183 mA h cm^{-3}) but suffers from a much larger volume expansion (430%) compared to Sb (293%), and slower reaction kinetics.[11]

The capacity retention of Mo–Sb film electrodes is presented in Fig. 3 for various currents, film thickness and with FEC electrolyte additive in the case of cycling with Na. The storage capacity when cycled with Na remains stable at about 330–340 mA h g^{-1} for about 30–40 cycles until it slowly declines with longer cycling. The use of thinner films (red and blue curves)

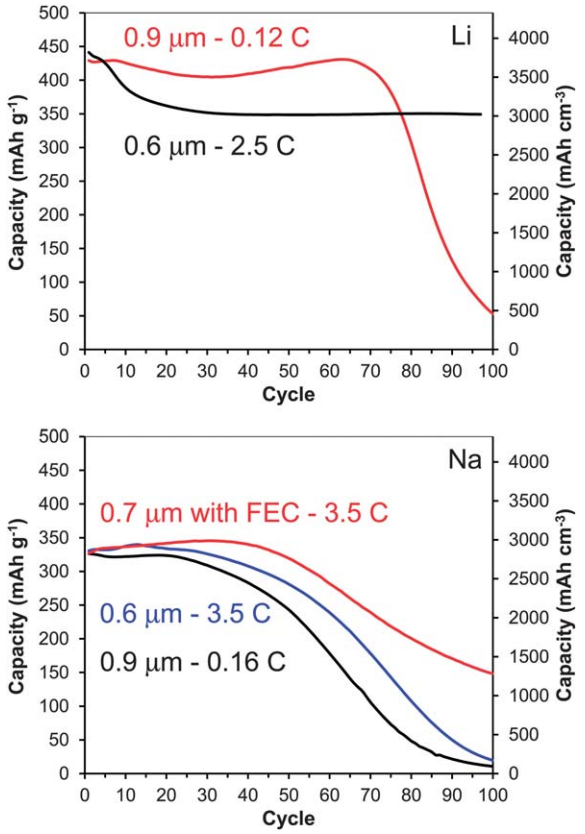

Fig. 3 Cycle life (reversible capacity) of Mo_3Sb_7 film electrodes for the reaction with Li and Na from 0 to 2 V at (a) low (40 µA cm^{-2}) and (b) high (630 µA cm^{-2}) currents. For Na, cycling with FEC additive was also conducted. The corresponding C-rate currents and film thicknesses are indicated.

somewhat improves the capacity retention compared to thicker films (black curve) even though the electrodes were cycled at a much higher rate. Interestingly, as observed earlier,[8,9,13,19,20] the use of FEC additive improves the capacity retention further (red curve). In contrast, cycling with Li provides higher and more stable capacity retention at about 430–440 mA h g^{-1} up to 70 cycles when cycling at low currents. At higher currents, the capacity initially declines and then stabilizes at 350 mA h g^{-1} for up to 100 cycles (ongoing measurement). The enhanced cycling behavior of pure Mo_3Sb_7 thick film indicates that the micron thick material can be reversibly cycled although undergoing tremendous volume expansion/shrinkage. The difference in capacity retention between Li and Na may be caused by the larger volume expansion of the Na-based electrodes as compared to their Li counterparts due to the larger size of Na ions. Indeed, the volume expansion expected for the formation of Li_3Sb from pure Sb is 135% for Li and 293% for Na, or a final to initial volume ratio of 2.35 and 3.93, respectively.[10] Here, assuming the composition and structure of Mo_3Sb_7, the formation of 3Mo + 7Li_3Sb should yield a final to initial volume ratio of 2.48 (expansion of 148%) whereas the formation of 3Mo + 7Na_3Sb should correspond to a much larger final to initial volume ratio of 4.0 (expansion of 300%).

Evidence of large morphological changes has been observed for pure In during the reaction with Li and Na.[18] Cycling was accompanied with an important decrease of the primary particle size and an increase of the secondary particle size, leading to the formation of isolated islands which slowly become electronically inactive.[18] For the reaction of Ge with Na, we have also evidenced that the film morphology importantly evolves upon cycling, which coupled with the electrolyte decomposition detrimentally affects the capacity retention.[19] It is well-known that not only the mechanical stress due to expansion/shrinkage of the active material influences the capacity retention but also the stability of the SEI film plays a crucial role.[11,18–23] Here the better cycling performance with Li could result from the lower volume expansion coupled with the more optimized electrolyte chemistry. Although it has been shown that the role of additives, such as FEC, can drastically improve the capacity retention of pure Sb,[8] SnSb,[12,13] AlSb[20] and Ge[19] electrodes due to the formation of different surface species,[10] the presence of 5 wt% FEC does not guarantee that the films will repeatedly cycle without capacity losses. From a practical point of view, the electrode material may instead ideally consist of nanosized particles embedded in a

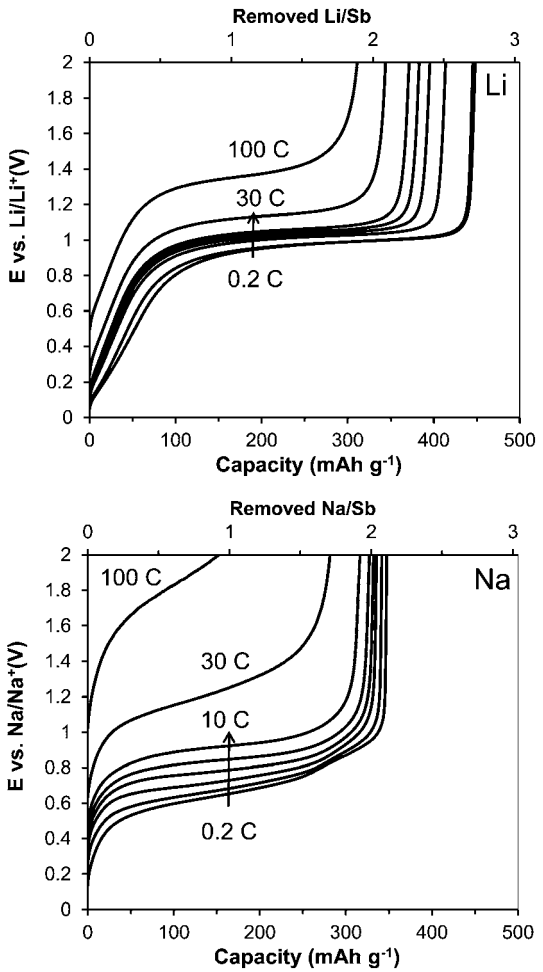

Fig. 4 Rate performance of 0.8 µm thick Mo_3Sb_7 film electrodes during charge (ion removal) measured from 0.2 C to 100 C-rate. All discharges were performed using constant current constant voltage steps with 1 C current until 0.005 V was reached, and held till the current dropped below 0.2 C.

(conductive) buffer matrix, and should be cycled with adequate electrolyte additives in sufficient quantities in order to promote the formation of a stable SEI film.

The rate performance of 0.8 μm thick films is presented in Fig. 4 during charging (ion removal). In both cases, extremely high rate performance is measured during the extraction of Li or Na ions with recovered capacities of around 300 mA h g^{-1} for Li and Na at 100 C and 30 C, respectively. During the removal of Li ions, the average plateau potential increases from around 0.98 V at C/5 to about 1.14 V at 30 C and up to 1.36 V at 100 C with delivered capacities of about 430, 340 and 310 mA h g^{-1}, respectively. During the extraction of Na ions, the average plateau potential increases from about 0.64 V at C/5 to 1.22 V at 30 C and up to 1.79 V at 100 C with delivered capacities of around 330, 280, 145 mA h g^{-1}, respectively. Obviously, the increase in overpotentials is smaller during Li ion removal, as also found for pure Sb films of comparable thickness.[10] The difference in reaction kinetics of Sb with Li and Na has been attributed to the slower solid-state diffusion of Na, as confirmed by the determination of diffusion coefficients and first principles calculations,[10] and is likely to be the main cause for the relatively lower rate performance of the Mo_3Sb_7 films with Na. Nonetheless, we would like to stress that both electrode systems have very good reaction kinetics with about 300 mA h g^{-1} delivered in only about 100 s at 30 C-rate. To summarize, the cycling and rate performance results highlight the high potential for Mo_3Sb_7 materials as anodes for both Li- and Na-ion battery applications.

The reaction of the electrode was investigated during discharge/charge for both ion systems using XRD (Fig. 5) and XPS (Fig. 6). The structure of the starting films characterized by XRD is amorphous (Fig. 5), as confirmed with SAED (Fig. 1b). The XRD pattern shows broad humps located around the strongest diffraction lines of Mo_3Sb_7, which suggests that the atomic short range ordering of the films is similar to that of crystalline Mo_3Sb_7. This similarity in structure is also suggested by the very close electrochemical profiles obtained during the reaction with Li (compare Fig. 2 and ref. 16) and the almost identical Sb/Mo ratios as determined by EDX chemical analysis. The changes in the bulk structure measured at full lithiation indicate that nanocrystalline Li_3Sb forms at 0 V (see Fig. S3†). After charging to 1.3 V, which corresponds to the quasi full-delithiation of the material, no diffraction lines are measureable except those from the Cu current collector. Unfortunately, due to the coverage of the samples with Kapton to protect the thin films from reacting in air, it is not possible to estimate if an amorphous phase matching the strongest lines of cubic Mo_3Sb_7 forms. In the case of the reaction with Na, the fully sodiated electrode material is amorphous and no evidence for the formation of crystalline or amorphous Na_3Sb is obtained. This result contrasts with the measurements on Cu_2Sb that forms nanocrystalline Na_3Sb domains at 0 V.[14] A similar situation is found for SnSb where no crystalline phases are formed during sodiation of the material[13] although the parent materials Sn[11] and Sb[8] can both crystallize during sodiation with Na. Finally, similarly to the reaction of Cu_2Sb with Na,[14] the material structure remains amorphous during the removal of Na ions (charging) at 1.2 V (Fig. 5).

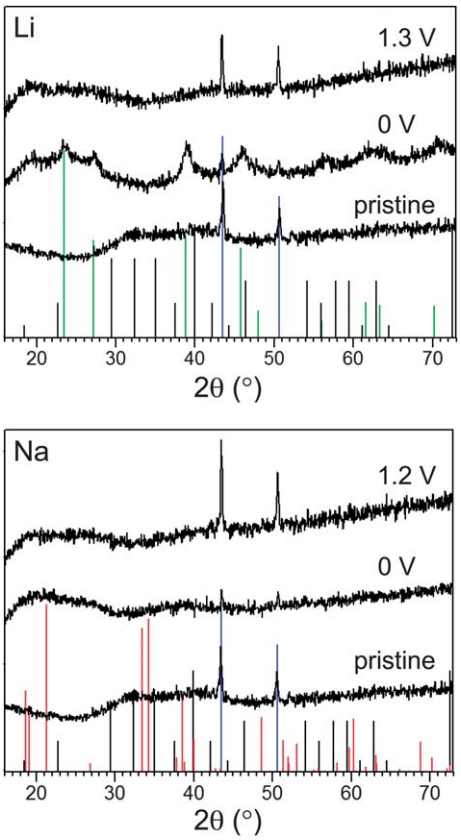

Fig. 5 X-ray diffraction patterns collected for a pristine Mo_3Sb_7 thin film and for Kapton-covered 3 μm thick film electrodes discharged to 0 V and charged to 1.3 or 1.2 V, respectively, for the reaction with Li and Na. Green, red, blue, and black vertical bars indicate the reference patterns for Li_3Sb, Na_3Sb, Cu and Mo_3Sb_7, respectively.

The surface chemistry analyzed with high resolution XPS is presented for the fully discharged/charged electrodes in Fig. 6. The stability of the SEI film formed onto anode and cathode surfaces is known to be essential for achieving safe and durable Li-ion batteries.[21–23] Generally, only the outer most 5 nm of the material can be probed by XPS when using Al or Mg K_α X-ray sources. Indeed, the photoelectron escape depth depends on the material properties, as well as the electron kinetic energy, which is related to the core level of origin.[24]

The surface of the pristine material is covered by various Sb- and Mo-oxides, as evidenced by the binding energies of Mo4p, Sb3d, and 4d core levels (Fig. 6), as well as the energies found for the Mo3p and 3d core levels (Fig. S4†). The surface of the electrode cycled in 1.2 M $LiPF_6$ in EC/DMC electrolyte is composed of inorganic compounds covered by an organic layer. Qualitatively, at full discharge (0 V), the surface is terminated, in descending order of concentration, by Li carbonates, esters or carboxylates, and ethers, as indicated by the binding energies of ~290, ~289 and ~286.5 eV in the C1s spectrum. A small quantity of LiF is measured according to the Li1s and F1s spectra and likely originates from species buried under the organic products. At full charge (2 V), the quantity of the species in the organic layer has importantly decreased and most of the surface is now composed of LiF evidenced by the Li1s, F1s and

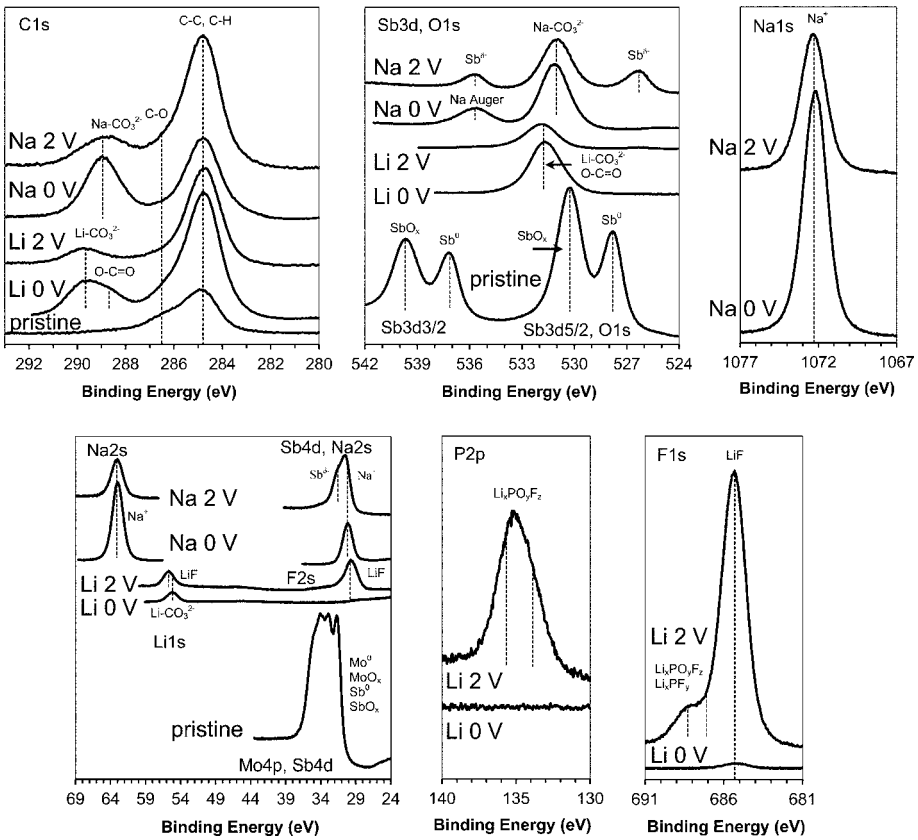

Fig. 6 X-ray photoelectron spectroscopy for a pristine Mo_3Sb_7 thin film and for thin film electrodes discharged to 0 V and charged to 2 V for the reaction with Li and Na. The Sb3d/O1s region for the 2 V charged Na electrode was acquired with Mg K_α radiation to avoid an important overlap with Na Auger lines.

F2s spectra, and some $Li_xPO_yF_z$ and Li_xPF_y species supported by the P2p spectrum. In both situations, the signals for Mo and Sb are not measured, which means that the SEI is relatively thick even at full charge (delithiation).

In contrast, the surface of the electrode cycled in 1 M $NaClO_4$ in PC electrolyte consists mostly of an organic layer. The organic products, especially at 0 V, are essentially made of Na carbonate species characterized by a C1s binding energy around 289 eV, matching Na_2CO_3 reference compound[11] and the surface chemistries measured for Sb[10] or Cu_2Sb[14] anodes. At full charge (2 V), the organic products quantity has decreased and the electrode surface is now visible as evidenced by the presence of Sb3d and 4d signals (Fig. 6) as well as signals of Mo, for example, Mo3d (Fig. S4†). This is quite different from the electrode surface cycled in the $LiPF_6$-based electrolyte and likely results from the quasi-absence of inorganic products in the case of cycling in $NaClO_4$-based electrolyte (only a marginal quantity of NaCl and $NaClO_4$ residue are measured; data not presented). The binding energies for Sb consistent with those expected for reduced species and likely correspond to Na_xSb compounds, as has been consistently observed for Sb and Cu_2Sb,[10,14] and for Sn electrodes.[11]

The poorer cycle life measured when cycling with Na (Fig. 3) may be related to the larger volume expansion with Na coupled with the formation of a less stable SEI layer.[21–23] For Na, as discussed above the absence of an inorganic layer when cycling with $NaClO_4$-based electrolyte results in the exposure of the electrode surface to the electrolyte. When cycling with $LiPF_6$-based electrolyte, however, the electrode surface is still protected at full delithiation (2 V) with an inorganic film that may minimize the side reactions with the electrolyte. In turn, the combination of a lower volume expansion and the presence of an inorganic SEI film can explain the better cycle life performance when cycling with Li. For Na, the beneficial role of FEC electrolyte additive on the cycle life previously reported for Sb-based electrodes[8,9,13,20] may be explained by the formation of an inorganic layer composed of NaF, as we evidenced using XPS on pure Sb films cycled with FEC additive.[10] Although Sb undergoes a much larger expansion with Na (293%) than with Li (135%),[10] the cycle life obtained with FEC additive was found to be superior,[8] as also measured here for Mo_3Sb_7 (Fig. 3). Hence, we relate the poorer cycle life measured without FEC additive to the absence of an inorganic passivation layer on the surface of the electrode, and suspect that this layer is crucial to achieve longer electrode operation. Nevertheless, it appears that the larger volume expansion is detrimental (compare cycling with Na *vs.* Li, Fig. 3) but should be mitigated by the preparation of electrode architectures consisting of, for example, embedded nanosized particles.

4 Conclusions

The properties of Mo_3Sb_7 thin film electrodes for Li- and Na-ion batteries, prepared by magnetron sputtering from a Mo_3Sb_7 target, have been reported. The starting films are amorphous with a Sb/Mo ratio very close to that of Mo_3Sb_7. The electrochemical

response during the reaction with Li indicates a similar response to that measured for crystalline Mo_3Sb_7 with reduction/oxidation peaks located around 0.85/1 V. In the case of the reaction with Na, the first discharge is characterized by a plateau at 0.4 V whereas the subsequent cycle shows conjugated discharge/charge sloping profiles at 0.5/0.65 V and 0.7/0.85 V. The reversible capacities of the electrode films are around 430 and 330 mA h g^{-1} for the reactions with Li and Na, respectively. Excellent rate performance and good cycling is obtained in both cases, although the reaction with Li shows the highest performances. Indeed, with Li, a reversible capacity of 310 mA h g^{-1} is obtained at 100 C accompanied by an increase in potential of only 0.4 V. During the reaction with Na, a reversible capacity of 280 mA h g^{-1} is measured at 30 C, accompanied by an increase in potential of 0.6 V. The study of the changes in bulk structure by XRD shows that Li_3Sb nanocrystallites can be formed at full discharge during the reaction with Li whereas the electrode remains amorphous with Na. This is somewhat analogous to the reaction of SnSb with Na but contrasts with the reaction of Cu_2Sb, which can form Na_3Sb nanodomains at full sodiation. The changes in surface chemistry as a function of potential highlight that the reaction with $LiPF_6$–EC/DMC electrolyte results in the formation of an inorganic layer composed of $LiF/Li_xPO_yF_z/Li_xPF_y$ covered, in descending order of concentration, by carbonate, ester or carboxylate, and ether organic species. In contrast, the reaction of the electrode with $NaClO_4$–PC electrolyte results in the formation of little inorganic products and mostly carbonate organic species, rendering the surface of the electrode partially exposed at full charge. We suspect that the exposure of the electrode surface detrimentally affects the cycle life performance. The results presented here demonstrate the good prospects of Mo_3Sb_7 as an electrode material for both Li-ion and Na-ion batteries.

Acknowledgements

This work was supported by the U.S. Department of Energy (DOE), Basic Energy Sciences (BES), Materials Sciences and Engineering Division (work at the University of Texas at Austin under award number DE-SC0005397). Microscopy research was supported *via* a user project supported by ORNL's Shared Research Equipment (ShaRE) User Program, which is also supported by DOE-BES.

References

1 M. Armand and J.-M. Tarascon, *Nature*, 2008, **451**, 652.
2 V. Palomares, P. Serras, I. Villaluenga, K. B. Hueso, J. Carretero-González and T. Rojo, *Energy Environ. Sci.*, 2012, **5**, 5884.
3 S.-W. Kim, D.-H. Seo, X. Ma, G. Ma and K. Kang, *Adv. Energy Mater.*, 2012, **2**, 710.
4 B. L. Ellis and L. F. Nazar, *Curr. Opin. Solid State Mater. Sci.*, 2012, **16**, 168.
5 P. Senguttuvan, G. Rousse, V. Seznec, J.-M. Tarascon and M. R. Palacín, *Chem. Mater.*, 2011, **23**, 4109.
6 S. Komaba, W. Murata, T. Ishikawa, N. Yabuuchi, T. Ozeki, T. Nakayama, A. Ogata, K. Gotoh and K. Fujimara, *Adv. Funct. Mater.*, 2011, **21**, 3859.
7 A. Ponrouch, A. R. Goñi and M. R. Palacín, *Electrochem. Commun.*, 2013, **27**, 85.
8 A. Darwiche, C. Marino, M. T. Sougrati, B. Fraisse, L. Stievano and L. Monconduit, *J. Am. Chem. Soc.*, 2012, **134**, 20805.
9 J. Qian, Y. Chen, L. Wu, Y. Cao, X. Ai and H. Yang, *Chem. Commun.*, 2012, **48**, 7070.
10 L. Baggetto, P. Ganesh, C.-N. Sun, R. A. Meisner, T. A. Zawodzinski and G. M. Veith, *J. Mater. Chem. A*, 2013, **1**, 7985.
11 L. Baggetto, P. Ganesh, R. P. Meisner, R. R. Unocic, J.-C. Jumas, C. A. Bridges and G. M. Veith, *J. Power Sources*, 2013, **234**, 48.
12 L. Xiao, Y. Cao, J. Xao, L. Kovarik, Z. Nie and J. Liu, *Chem. Commun.*, 2012, **48**, 3321.
13 A. Darwiche, M. T. Sougrati, B. Fraisse, L. Stievano and L. Monconduit, *Electrochem. Commun.*, 2013, **32**, 18.
14 L. Baggetto, E. Allcorn, A. Manthiram and G. M. Veith, *Electrochem. Commun.*, 2013, **27**, 168.
15 L. Baggetto, J.-C. Jumas, J. Górka, C. A. Bridges and G. M. Veith, *Phys. Chem. Chem. Phys.*, 2013, **15**, 10885.
16 D. Appelstone, S. Yoon and A. Manthiram, *J. Phys. Chem. C*, 2011, **115**, 18909.
17 Z. Bukowski, D. Badurski, J. Stepien-Damm and R. Troc, *Solid State Commun.*, 2002, **123**, 283.
18 S. A. Hawks, L. Baggetto, C. A. Bridges and G. M. Veith, *J. Power Sources*, 2014, submitted.
19 L. Baggetto, J. K. Keum, J. F. Browning and G. M. Veith, *Electrochem. Commun.*, 2013, **34**, 41.
20 L. Baggetto, M. Marszewski, J. Górka, M. Jaroniec and G. M. Veith, *J. Power Sources*, 2013, **243**, 699.
21 D. Aurbach, *J. Power Sources*, 2000, **89**, 206.
22 K. Xu, *Chem. Rev.*, 2004, **104**, 4303.
23 K. Edström, T. Gustafsson and J. O. Thomas, *Electrochim. Acta*, 2004, **50**, 397.
24 S. Hofmann, in *Practical Surface Analysis*, ed. D. Briggs and M. P. Seah, John Wiley & Sons Ltd, Chichester, 2nd edn, 1990, vol. 2, ch. 4, pp. 151–152; M. P. Seah, in *Practical Surface Analysis*, ed. D. Briggs and M. P. Seah, John Wiley & Sons Ltd, Chichester, 2nd edn, 1990, vol. 2, ch. 5, pp. 207–208.